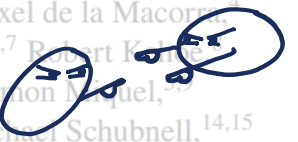


Galaxies point at each other and mess up measurements of the Universe

Intrinsic Alignment as an RSD Contaminant in the DESI Survey

Claire Lamman ,^{1*} Daniel Eisenstein,¹ Jessica Nicole Aguilar,² David Brooks,³ Axel de la Macor ,⁴
 Peter Doel,³ Andreu Font-Ribera ,⁵ Satya Gontcho A Gontcho,² Klaus Honscheid,^{6,7} Robert Kehoe ,⁸
 Theodore Kisner ,² Anthony Kremin ,² Martin Landriau ,² Michale Levi ,² Ramon Martínez ,⁹
 John Moustakas ,¹⁰ Nathalie Palanque-Delabrouille ,^{2,11} Claire Poppett,^{2,12,13} Michael Schubnell,^{14,15}
 Gregory Tarlé ,¹⁵



¹Center for Astrophysics | Harvard & Smithsonian, 60 Garden Street, Cambridge, MA 02138, USA

²Lawrence Berkeley National Laboratory, 1 Cyclotron Road, Berkeley, CA 94720, USA

³Department of Physics & Astronomy, University College London, Gower Street, London, WC1E 6BT, UK

⁴Instituto de Física, Universidad Nacional Autónoma de México, Cd. de México C.P. 04510, México

⁵Institut de Física de Altres Energies (IFAE), Institut d'Estudis Avançats de Ciència i Tecnologia, Campus UAB, 08193 Bellaterra Barcelona, Spain

⁶Center for Cosmology, Cosmology & Physics, The Ohio State University, 191 West Woodruff Avenue, Columbus, OH 43210, USA

⁷Department of Physics, The Ohio State University, 191 West Woodruff Avenue, Columbus, OH 43210, USA

⁸Department of Physics, Southern Methodist University, 3215 Daniel Avenue, Dallas, TX 75275, USA

⁹Institució Catalana de Recerca i Estudis Avançats, Passeig de Lluís Companys, 23, 08010 Barcelona, Spain

¹⁰Department of Physics and Astronomy, Siena College, 515 Loudon Road, Loudonville, NY 12211, USA

¹¹IRFU, CEA, Université Paris-Saclay, F-91191 Gif-sur-Yvette, France

¹²Space Sciences Laboratory, University of California, Berkeley, 7 Gauss Way, Berkeley, CA 94720, USA

¹³University of California, Berkeley, 110 Sproul Hall #5800 Berkeley, CA 94720, USA

¹⁴Department of Physics, University of Michigan, Ann Arbor, MI 48109, USA

¹⁵University of Michigan, Ann Arbor, MI 48109, USA

Accepted XXX. Received YYY; in original form ZZZ

INFORMATION-DENSE SUMMARY

ABSTRACT

We measure how the orientations of galaxies correlate with large structures of matter in the Universe. DESI is surveying galaxies, but there is a bias in the orientations of galaxies they choose to observe. We also estimate this bias, and explore how these two effects combine to mess up DESI's measurements of how matter is distributed on large scales (don't worry if this effect isn't immediately obvious!).

Key words: methods: data analysis –cosmology: observations – large-scale structure of Universe –– cosmology: dark energy

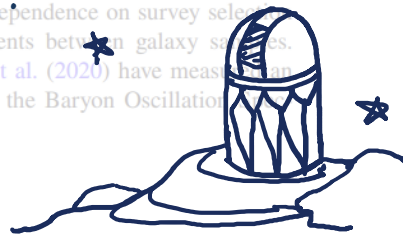
INTRODUCTION

INTRODUCTION

The Universe is like old milk. It started out smooth and uniform, but gets clumpier over time. By measuring the structure of mass clumps and how it changes, we learn about the components which create it –i.e. gravity and dark energy.

* craig.lamman@cfa.harvard.edu

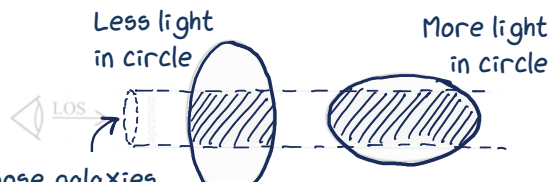
To fully utilize RSD measurements in large spectroscopic galaxy surveys, one of their important biases must be understood: intrinsic galaxy alignment (IA). The principal axes of galaxies can be intrinsically aligned with each other (II correlation) and with the underlying density, δ . In addition to the orientation-dependent bias, the orientation-dependent elevation bias and galaxy orientations are also correlated with the tidal field, ζ_2 is directly affected by DESI is doing this by mapping out 40 MILLION galaxies. To make the best use of all this data and get the most accurate measurements possible, we need to understand even the smallest sources of error. Hirata (2009) used linear models of tidal alignment and orientation-dependent bias to predict the effect of IA on RSD measurements. This effect can affect RSD measurements by as much as 10%. This effect is highly survey-dependent due to its strong dependence on survey selection and the differences in tidal alignments between galaxy samples. Martens et al. (2018) and Obuljen et al. (2020) have measured the anisotropic galaxy assembly bias in the Baryon Oscillation



2

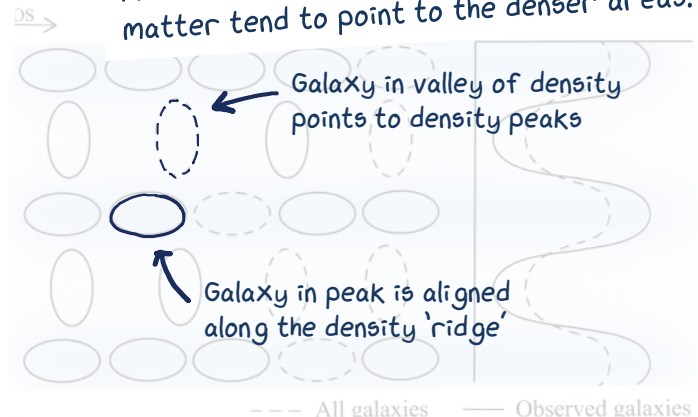
DESI is more likely to observe an elliptical galaxy which is pointed at us, because its light is more concentrated on the sky

Galaxy light that falls within our aperture



We choose galaxies based on how much of their light is in an aperture (circle on the sky)

Galaxies tend to point along strands of matter. Galaxies not in the strands of matter tend to point to the denser areas.



This figure explains the key idea of my paper and what we're trying to measure.

A bias in the orientations of galaxies we choose to observe + Galaxy orientation correlated with large structures of matter = A bias in how we measure the large structures of matter

troscopic Survey (BOSS). Since the velocity dispersion of elliptical galaxies will have the maximum concentration of light in the sky when the major axis is pointed at the observer. In this case, more of the light falls within an aperture and it is more likely to be included in DESI's four magnitude selection. The cartoon on the right shows galaxies with maximum tidal alignment along density ridges which are parallel to the LOS. These galaxies are more likely to point toward the higher density regions. In this case, DESI is more likely to select galaxies in denser regions, resulting in an amplification of this density mode. The opposite effect happens for filaments which are perpendicular to the LOS (not shown here; see Figure 1 of Martínez et al. 2021), and we are more likely to select galaxies in filaments which are perpendicular to the LOS, and we are less likely to select galaxies in filaments which are parallel to the LOS, leading to an amplification of the RSD signal.

As a Stage IV survey, it is necessary to not only detect, but quantify these biases for the Dark Energy Spectroscopic Instrument (DESI). DESI is in the midst of a 5-year survey measuring spectra of over 40 million galaxies within 16,000 deg². (DESI Collaboration et al. 2016; DESI Collaboration et al. 2022).

Success in the selection of a galaxy based on its redshift depends on target surface brightness. This is true for a large survey like DESI, which prioritizes survey speed at the cost of higher signal-to-noise. To impose this explicitly, DESI adopts a surface brightness-dependent cut: limiting the magnitude within an aperture instead of total magnitude. This selection creates systematic errors related to surface brightness bias in the 3D orientation of galaxies. Galaxies with a pole-on orientation have a higher surface brightness and are more likely to be selected. Since galaxies with tidal alignments tend to point along strands of matter, this is not a new idea, but DESI may be the first survey of its kind where it's actually an issue. This is not a new idea, but DESI may be the first survey of its kind where it's actually an issue. This is not a new idea, but DESI may be the first survey of its kind where it's actually an issue.

About 2% of DESI targets are LRGs, which fall in the redshift range 0.8 – 1.0 (Zhou et al. 2021). These high-redshift galaxies are affected by aperture-based selection because they have larger angular sizes than Emission Line Galaxies (ELGs) (see Figure 1). This is not a new idea, but DESI may be the first survey of its kind where it's actually an issue.

LRGs as the DESI sample most likely to be substantially biased by these alignments, although our methods would also work for ELGs.

The two effects that combine to create this bias, GI alignment and selection-induced polarization, can both be estimated and used to calibrate the quadrupole ξ_2 . We will use the three-point correlation function $\xi_{\ell\ell}$ measured in the plane of the sky using shapes from the DESI Legacy Imaging Survey (Ley et al. 2019) to isolate the signal of intrinsic polarization. We do this via photometric redshifts, model DESI's orientation-dependent selection function, and put our detection in context of ξ_2 via a linear tidal model. As an additional test, we use the ABACUSSUMMIT cosmological simulations to reproduce an aperture-based selection and measure the effect on ξ_2 .

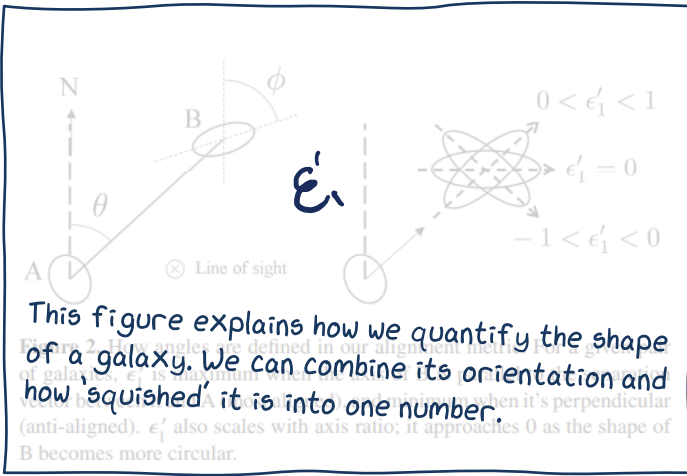
HOW WE GOT THE DATA

2.1 Imaging

Our measurements of GI alignment were made with LRGs from the Legacy Imaging Survey (DB2; DESI Collaboration et al. 2019). This is the catalog DESI uses to select its targets, and contains imaging in three bands (g, r, i) and optical spectroscopy in the $\lambda > 4000 \text{ nm}$ extra galactic sky. It also includes photometry from the Wide-field Infrared Survey Explorer, which contains J , H , and K_s filters that are correlated with the optical bands.

The source of each target (after PSF deconvolution) is modeled as several light profiles at the same time, using several models (Tresse et al. 2010). Based on the χ^2 values, we pick the best parameters from the best fit out of these models: exponential disk, de Vaucouleurs, and Sersic. This is different from DESI's default selection, which includes PSF and round-exponential fits, and a normalized χ^2 criteria to avoid over-fitting bright targets as round-exponentials. These models were avoided for our measurements, as circles have no distinguishable orientation.

Quality cuts were applied to target declinations $\delta > -30^\circ$ and galactic latitudes $b > 20^\circ$. The W1 color correlates well with redshift, so we used this color for the pair selection and weighting scheme.



detailed in 3.2. To conform with these weights, color outliers were removed by requiring $1 < r - W_1 < 4.5$. Our final sample contained 17,500 nearby LRGs. Generally, the redder a galaxy is, the further away it is. Since DESI has measured the distances to some galaxies already, we can calibrate a distance vs color relationship and use it to guess the distances to the galaxies which haven't yet been measured. This is done by fitting a linear regression to the spectroscopic redshifts from the DESI Survey Validation (SV) observations. SV is designed to represent the full survey and is used to assess the performance of the DESI pipeline. It contains 17,500 galaxies, which comprises of quality observations taken from 14 December 2020 through 10 June 2021. From this we selected 133,924 LRGs with colors $0.6 < r - z$ and $1.5 < r - W_1 < 4.5$, and redshifts $0.001 < z < 1.4$.

3 INTRINSIC ALIGNMENT SIGNAL

3.1 Alignment Formalism

HOW WE MEASURE CORRELATIONS OF GALAXY SHAPES The alignment signal on the sky is quantified with the degree to which a galaxy is aligned with, and stretched along, a separation vector between it and another galaxy. Measuring this as a function of the separation vector's magnitude for many galaxy pairs is a way to quantify the alignment of LRGs to the underlying tidal field.

Here, we treat every picture of a galaxy as an oval. This section describes how we use math to represent:

$\epsilon = \frac{a - b}{a + b}$ where a and b are the primary and secondary axis of the 2D ellipse, and ϕ is the orientation angle of the primary axis, measured East of North. We define the ellipticity of a galaxy B relative to another galaxy A using the primary axis angle, ϕ_B , and its position angle relative to A , θ_{BA} , also measured East of North.

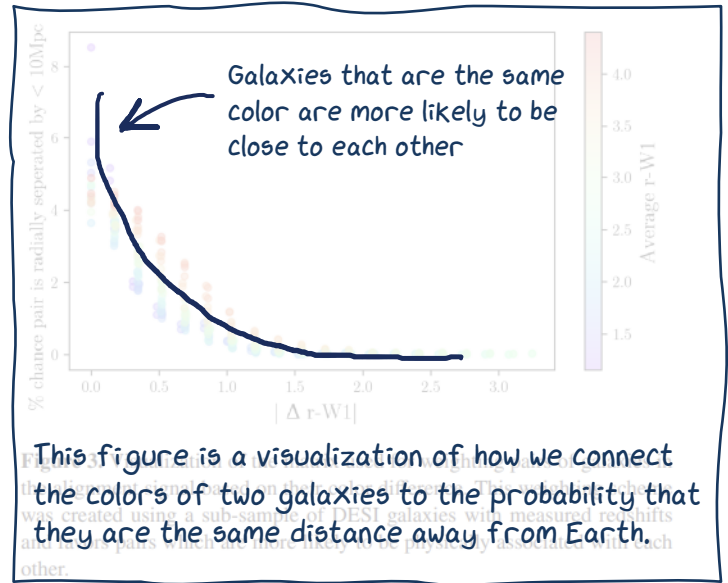
$$\theta' = \phi_B - \phi_A \quad (2)$$

2. How much that galaxy points towards other galaxies This gives us a relative ellipticity, for which we measure the real component:

$$\epsilon' = \frac{a_B - b_B}{a_B + b_B} \exp 2i\theta' \quad (3)$$

$$\epsilon'_1 = \text{Re}(\epsilon') = |\epsilon'| \cos \theta' \quad (4)$$

This measurement is averaged over many pairs of galaxies at varying separations to obtain $w_X(R)$, the 2D shape-density correlation.



This figure is a visualization of how we connect the colors of two galaxies to the probability that they are the same distance away from Earth. It shows the fraction of randomly paired galaxies that are within 10 Mpc of each other as a function of their color difference, $|r - W_1|$. The distribution is centered around zero, with a higher density of pairs having the same color ($|r - W_1| \approx 0$) and a lower density for pairs with different colors. The color bar indicates the average $r - W_1$ value for each data point.

3.2 Color Weighting

Just because two galaxies are in the same place in the sky, doesn't mean they're actually close to each other! As our signal is diluted by the survey volume, its dilution is from pairs of galaxies with large radial separations. At the time of this paper, we do not have spectra of all of the imaged galaxies and cannot lift the weight off every color. We are more likely to be physically associated a higher weight in the alignment signal, we created a weighting scheme based off of their $r - W_1$ colors.

Using the redshifts DESI has measured so far, detailed in Section 2.2, we separated galaxies into 20 bins of $r - W_1$ color. We then calculated the fraction of galaxies which are radially separated by less than 10 Mpc for every combination of two colors based on their redshift difference and assuming the Hubble flow. The resulting lookup matrix was then used as a weight when averaging the alignment signal from individual pairs (Figure 3).



3.3 Intrinsic Alignment

The catalog was divided into 100 groups based on declination, and then each of those into 10 groups based on right ascension, resulting in 100 sky regions with an equal number of galaxies in each, 1.8 million. We measured the projected alignment of neighboring galaxies relative to each galaxy in each region. This was averaged over 20 bins of angular separation, resulting in 100 determinations of the IA signal. The average and standard error of these 100 measurements at each separation is our projected IA measurement, $w_X(R)$ ¹.

Our final determination of $w_X(R)$ for DESI LRGs is displayed in Figure 4. The signal already agrees with our measurement of projected IA in the Abacus Mock from Section 4, which did not include any matter. The LRGs have more complex orientations. The similarity between the alignment in LRGs and raw halo shapes is likely a coincidence due to two opposing effects: halo orientations are more aligned than LRGs, but LRGs are more elongated than w_X , but are rounder than LRGs, which dilutes w_X . The LRG measurements of w_X in each angular bin are statistically independent of each other, as demonstrated in Figure 5. The scatter between the 20 bins of radial separation (Figure 5)

Even though we don't know the distances to these galaxies (yet), we can use their colors and try to only make measurements of galaxies which are actually close to each other.

¹ code available here: github.com/cmlamman/ellipse_alignment

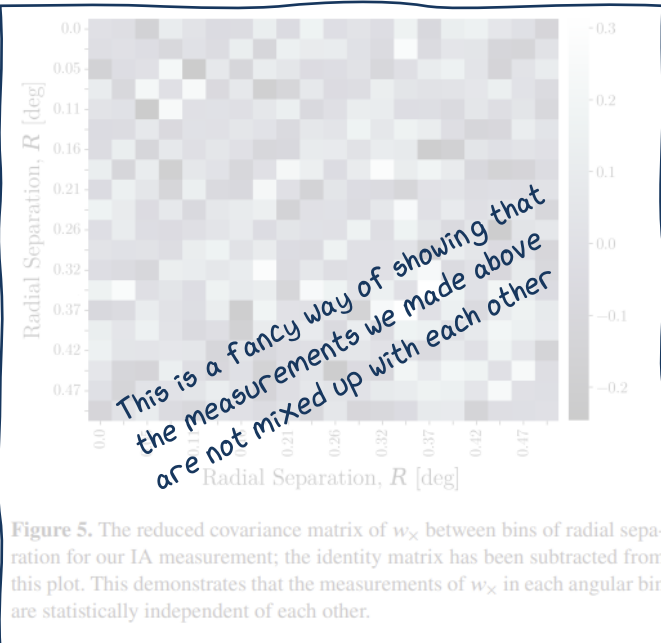
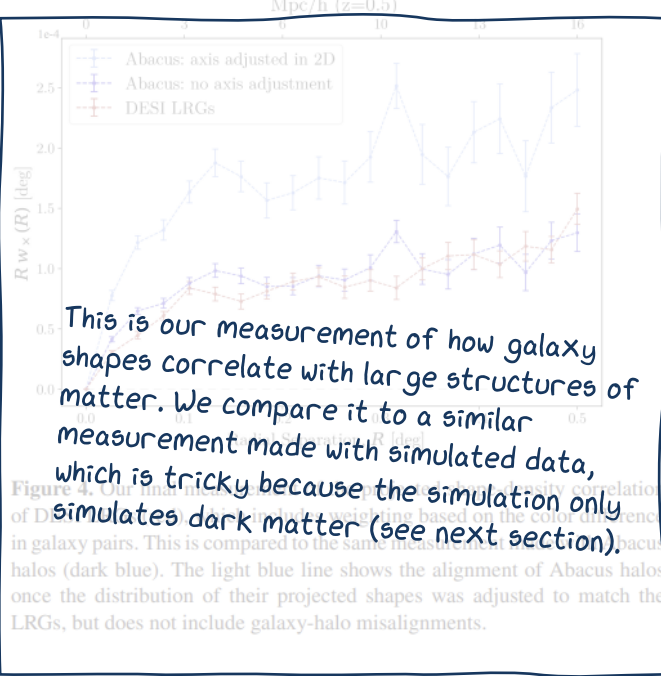


Figure 5. The reduced covariance matrix of w_x between bins of radial separation for our IA measurement; the identity matrix has been subtracted from this plot. This demonstrates that the measurements of w_x in each angular bin are statistically independent of each other.

3.4 Weak Lensing

DARN GRAVITY WARPS LIGHT
Lensing: it makes JWST images pretty but it makes my data pretty messy.

Since we only measure the shape of one galaxy in each pair, weak lensing is only present when the measured galaxy is in front of the central one. Therefore a simple way to isolate the weak lensing and IA signals is to set restrictions on the radial separations of pairs. In this work, we limit ourselves to pairs where the central galaxy is the primary axis of the pair. This allows us to measure the alignment for sets of pairs with various color restrictions (Figure 7), without having to only measure the shape of galaxies relative to the central one. This is important for our IA measurement using color weighting. The signal from only measuring galaxy shapes in a telescope are slightly warped.

In the first part of this section, I explain a neat way we can use galaxy colors to separate the signal caused by real galaxy shapes from the signal caused by lensed galaxy shapes.

To check whether the lensing signal is consistent with expectations we consider the following approximate model. The net effect of weak lensing on the alignment of a source galaxy is due to the gravitational shear on the sky:

$$\gamma_t = \frac{\bar{\Sigma}(< r) - \Sigma(r)}{\Sigma_{\text{crit}}} \quad (5)$$

where $\bar{\Sigma}(< r)$ is the average surface density within some transverse distance r . Here, $R_{\text{lens}} = 10 \text{ Mpc}/h$ is the correlation length for DESI clustering ($R_{\text{lens}} = 10 \text{ Mpc}/h$, 2020), $\beta = 1.0$ is the clustering bias for DESI LRGs (Zehavi et al. 2021), and $\rho_0 = 2.68 \times 10^{-30} \text{ g cm}^{-3}$ is the critical matter density of the Universe from Planck 2018 (Cosmology Working Group 2020). D_S , D_L , and D_{LS} are the distances to the source, distance to the lens, and distance between them, respectively. Assuming the correlation function goes as $\xi(r) = r_0^2 \rho_0 / \beta r^\alpha$,

$$\bar{\Sigma}(< r) = \frac{2\pi}{r} r_0^2 \frac{\rho_0}{\beta} \quad (6)$$

$\Sigma(r)$ is the average surface density at r

$$\Sigma(r) = \frac{r_0^2}{r} \pi \frac{\rho_0}{\beta} \quad (7)$$

and Σ_{crit} is the critical mean density, above which the light of a source is split into multiple images.

$$\Sigma_{\text{crit}} = \frac{c^2}{4\pi G} \frac{D_S}{(1+z_l) D_L D_{LS}} \approx \frac{c^2 D_S}{4\pi G D_L D_{LS}} \quad (8)$$

In the second part of this section, we lay out the theory for how we can predict what effect lensing will have on our signal.

$$\gamma_t = \frac{a-b}{a+b} e^{2i\phi} \quad (9)$$

where ϕ is the azimuthal angle of the source galaxy's primary axis with respect to the lens (Elmer et al. 2018).

$$\bar{\epsilon}_1' = \frac{\bar{\gamma}_t}{-2} \quad (10)$$

To measure this in our sample, we used photometric redshifts to estimate $D_S/D_L D_{LS}$ for every pair of galaxies, and average the result. We used a simple, linear fit of our DESI spectroscopic sample for redshifts:

$$z = 0.25(r - W_1) - 0.02 \quad (11)$$

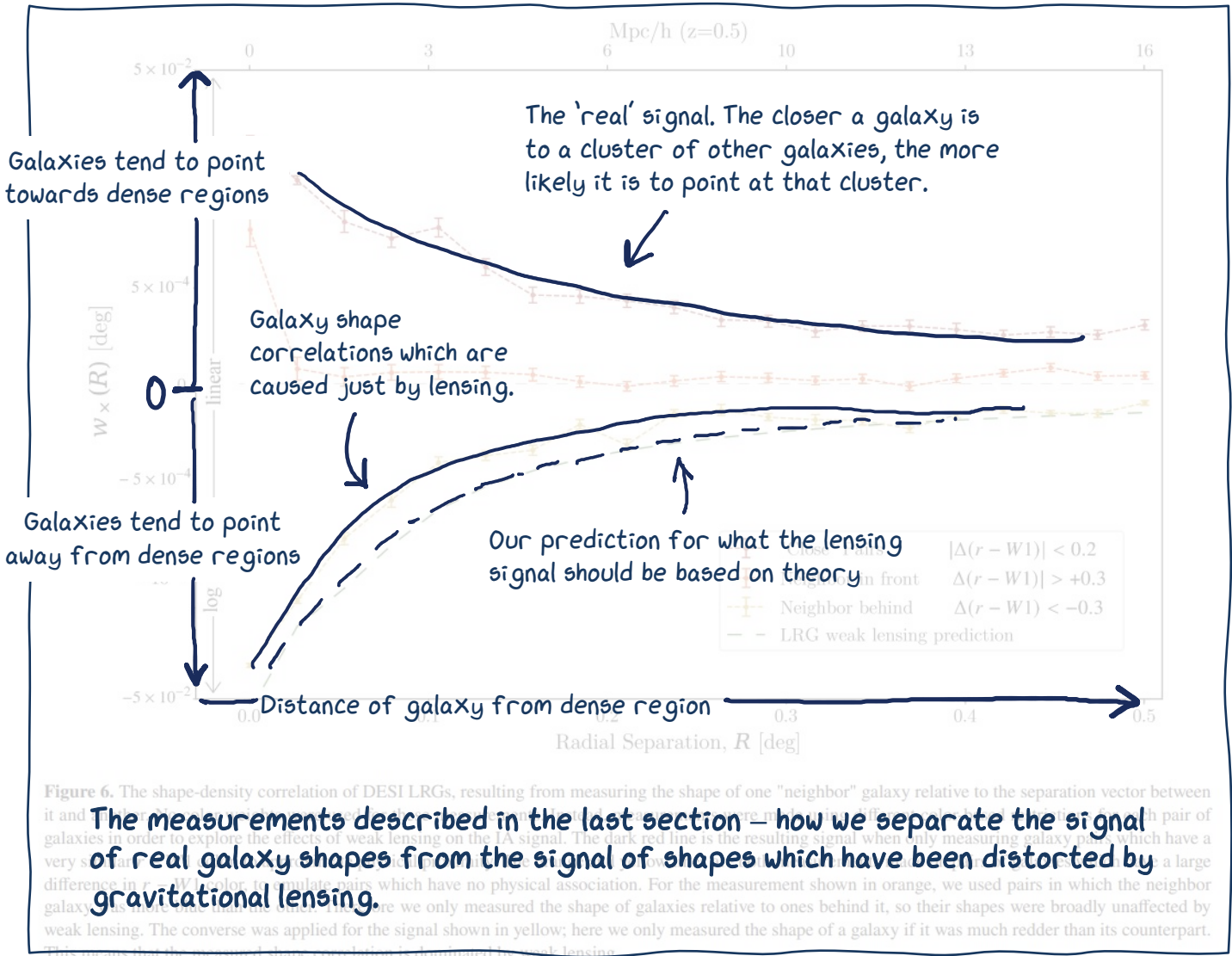
The resulting lensing estimation is shown in Figure 6 and agrees well with the IA measurement made when limiting to pairs we expect are only affected by lensing. This final IA signal is likely still diluted by weak lensing. However we did not develop a more sophisticated adjustment for lensing, as DESI's first year of spectra will allow us to sufficiently isolate physically-associated pairs.

4 IA WITH ABACUS MOCK CATALOG

To contextualize the measured IA signal, we built a mock catalog from the AbacusSummit CompASO halo catalog (Hadzhiyska et al. 2021). AbacusSummit is a suite of large, high-accuracy, high-resolution cosmological simulations made with the code N-body code GADGET (Springel 2001; Springel & Hernquist 2003; Amara et al. 2021). We used halos from a box moving 2000 h^{-1} Mpc sides, simulated at $z=0.725$.

Turn page to see what we did with a dark matter simulation!





COMPARING TO SIMULATED DATA

We mapped the halos' comoving positions to redshift and sky coordinates by placing an observer $1700 h^{-1}$ Mpc away from the center of the box along the x -axis. To have an even sky distribution

This section is all about how we reproduced our measurements of real galaxies with a simulation. This is tricky because the simulation only includes dark matter, so we're comparing big blobs of invisible matter to tiny bits of visible matter.

We then selected the largest halos to match both the LRG density of our DESI sample (with a matching $0.05 < (h^{-1}\text{Mpc})^3 < 0.1$) and the redshift distribution from DESI spectra. Our final mock catalog contains 766,341 halos.

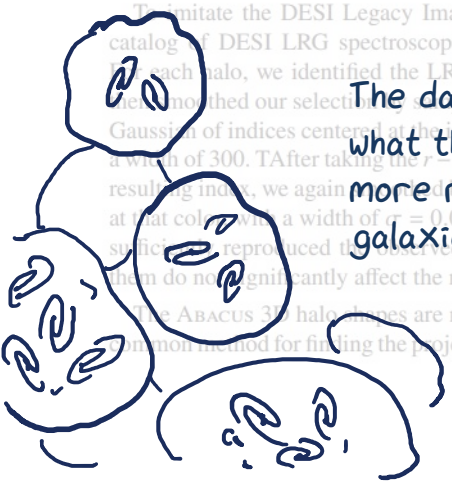
To initiate the DESI Legacy Imaging Survey colors, we used a catalog of DESI LRG spectroscopic redshifts, sorted by redshift. For each halo, we identified the LRG with the closest redshift. We then smoothed our selection using a Gaussian filter with a width of 300. TAfter taking the $r - W1$ color of the LRG with the resulting index, we again smoothed it with a Gaussian filter at that color with a width of $\sigma = 0.03$. These smoothing parameters suffice to reproduce the observed data spread, and variations of them do not significantly affect the measured alignment signal.

The ABACUS 3D halo shapes are modeled as triaxial ellipsoids. A common method for finding the projected axis ratios of ellipsoids can

be found in Binney (1985). For measuring the alignment of galaxy shapes, we additionally need the orientation angle of the projected shape. Therefore, we adapted the method derived in Gendwill & Stufler (1984) to project ellipsoids onto the celestial sphere. Our process for obtaining the axis ratio and orientation of an ellipsoid is described in detail in Appendix A. We then map the projected ellipsoids onto the celestial sphere and calculate the projected axis ratios of the ellipsoids. We adjust each axis ratio, $b/a = d$, with the empirical function:

$$d' = 1 + 1.1(d - 1) - 2.035(d - 1)^2 + 1.76(d - 1)^3 \quad (12)$$

This function correctly reproduces the number of observed axis ratios which fall in bins between 0 and 1. We made no adjustments for the orientation of the ellipsoids. Using the same color-weighting scheme as described in Section 3.1, we find that the projected axis ratios of our resulting halo catalog are in good agreement with the empirical function of our resulting halo catalog. The result can be seen in Figure 4. The higher amplitude is likely due to the simulation not including the effects of weak lensing and the higher degree of alignment in halos compared to galaxies. Tenneti et al. (2014) estimates large, central galaxies at DESI redshifts to be misaligned with their host halo by an average



of around 10-20°. This propagates to a w_X signal that is 75-94% of the same signal measured directly.

USING MATH TO CONNECT ALL THE PARTS OF THIS PAPER

5 MODELING ALIGNMENT - ξ_2 CORRELATION

5.1 Linear Tidal Model

We adopt a linear tidal model to connect IA and DESI's shape selection bias with the quadrupole of the correlation function, ξ_2 . This approximation assumes that the projected shapes of galaxies are linearly related to the projected density distribution and holds for LRGs above projected separations of $10 h^{-1} \text{Mpc}$ (Cattelan & Porciani 2001; Hinsen et al. 2010). We also assume that the projected density is

At this point, we've measured how the shapes of galaxies correlate with the large, underlying structure of matter. But how exactly is this measurement connected with the galaxy statistics that DESI cares about?

We model the mean 2D ellipticity of a triaxial galaxy as τT_{ij} , where the axis lengths behave as $1+\tau I$. For this derivation, we assume that 2D projections of such galaxies behave as the 2D projection of these lengths. The mean eccentricity tensor must also be traceless, so for a projection with $\alpha, \beta = \{x, y\}$, the projected ellipticity is given as $\epsilon_{\alpha\beta} = \tau(T_{\alpha\beta} + T_{zz})$, where we used $T_{xx} + T_{yy} = -T_{zz}$.

Using Fourier-space conventions and the matter power spectrum $\langle \tilde{\rho}(\vec{q}) \tilde{\rho}^*(\vec{k}) \rangle = (2\pi)^3 P(\vec{k}) \delta^D(\vec{q}-\vec{k})$, we have the tidal tensor model:

$$T_{ij}(\vec{r}) = \left(\partial_i \partial_j - \frac{\delta_{ij}^K}{3} \nabla^2 \right) \int \frac{d^3 k}{(2\pi)^3} \tilde{\phi}(\vec{k}) e^{i\vec{k}\cdot\vec{r}}$$

Using a basic* model, we get this relation:

$$= \int \frac{d^3 k}{(2\pi)^3} \left(\frac{k_i k_j - \delta_{ij}^K k^2 / 3}{k^2} \right) \tilde{\rho}(\vec{k}) e^{i\vec{k}\cdot\vec{r}}$$

5.2 Shape-Density Correlation

To consider the correlation of galaxy ellipticity with surface density, we begin with the expression for the projected fractional overdensity for a survey of functional depth L and uniform mean density ρ :

The "fake" RSD signal \propto

$$\Sigma(R) = \frac{1}{L} \int dz \rho(R, z)$$

where \hat{z} is along the LOS and \vec{R} is projected separation. L is a measure of how far along the LOS we average when measuring ϵ_{LRG} . As our survey is not homogeneous, we generalize L to an i.e. – the more galaxy correlation we see, and the more bias there is in galaxy shapes, the bigger problem we have. B_d .

$$L = B_d \frac{\Sigma_{B1} \Sigma_{B2} \Sigma_i \Sigma_j w(i, j)}{\Sigma_{B1} \Sigma_i \Sigma_j w(i, j)}$$

The projected ellipticity is $\hat{R}_\alpha \epsilon_{\alpha\beta} \hat{R}_\beta$. For the average, we can just consider the $\hat{R} = \hat{x}$ direction. The shape-density correlation projected onto the plane of the sky is then given as

$$w_X(R) = \langle \epsilon_{xx} \Sigma(R\hat{x}) \rangle = -\frac{\tau}{L} \left\langle T_{yy} \int dz \rho(R\hat{x}, z) \right\rangle$$

We compute and simplify this expression (Appendix B1) to

$$w_X(R) = \frac{\tau}{3L} R^2 \frac{d}{dR} \left[\frac{1}{R^2} \Psi(R) \right]$$

* Do NOT let this word fool you. It was the simplest model we could use, but oohhh man was it a pain to figure out.

where we introduce

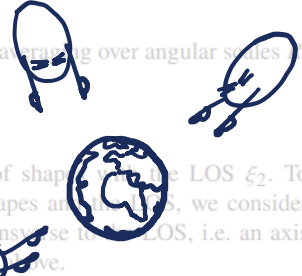
$$\Psi(R) = -\frac{d\Phi}{dR} = \int \frac{K}{2\pi} \frac{dK}{P(K)} J_1(KR) \quad (18)$$

K is 2D Fourier Space, P is the power spectrum, and J_1 is the first Bessel function.

τ can be inferred from our measurement of the shape-density correlation, $\langle \epsilon_{xx} \Sigma(R\hat{x}) \rangle$, showing that the LOS shape and ξ_2 are correlated. We estimate τ as

$$\tau_{obs} = \frac{3Lw_X}{R^2 \frac{d}{dR} \left[\frac{1}{R^2} \Psi \right]}, \quad (19)$$

with our IA measurement, w_X , and averaging over angular scales L .



5.3 Shape - ξ_2 Correlation

Next, we turn to the correlation of shape with the LOS ξ_2 . To obtain the relation between 3D shapes and the LOS, we consider shapes viewed from a direction transverse to the LOS, i.e. an axis perpendicular to the projection axis. Since we define ξ_2 as $\xi(r, \mu) = \sum_\ell \xi_\ell(r) L_\ell(\mu)$, with μ the cosine of the angle to the LOS, ξ_2 is given as

$$Q(r) = 5 \int \frac{d^2 \vec{r}}{4\pi} \rho(\vec{r}) L_2(\mu) \quad (20)$$

No, this doesn't mean Earth is special. This is not a real property of the Universe. It's caused by how DESI (located on Earth) chooses its targets, and is explained more later.

Considering projections along \hat{x} also yield $T_{zz}/2$ as the only $m=0$ support.

How much the shapes of galaxies correlate with large-scale structure	X	How much galaxies in the survey tend to be pointed towards Earth
--	---	--

$$\langle \epsilon_{zz} Q(r) \rangle = -\frac{\tau}{3} \int \frac{q^2}{\Sigma_r^2} P(q) j_2(q), \quad (22)$$

This expression is averaged over radial bins of the correlation function, resulting in averages of $j_2(qr)$.

5.4 Bias on ξ_2

We expect the mean shape to be elongated along the LOS due to DESI's target selection, i.e. a non-zero mean ϵ_{zz} (Section 6). We call this LOS polarization ϵ_{LRG} .

Assuming ϵ_{zz} and the quadrupole signature Q are Gaussian distributed, correlated, random variables, a non-zero $\langle \epsilon_{zz} \rangle$ will result in a non-zero mean $Q(r)$ as

$$\langle Q \rangle = \langle \epsilon_{zz} \rangle \frac{\langle \epsilon_{zz} Q \rangle}{\langle \epsilon_{zz}^2 \rangle}. \quad (23)$$

where the expectation values come from summing over each galaxy. From our tidal model,

$$\langle \epsilon_{zz}^2 \rangle = \frac{\tau^2}{4} \langle T_{zz}^2 \rangle \quad (24)$$

$$= \frac{\tau^2}{45} \int \frac{q^2 dq}{2\pi^2} P(q). \quad (25)$$

This is the variance in the density field σ^2 , hence $\langle \epsilon_{zz}^2 \rangle = \tau^2 \sigma^2 / 45$.

Combining the above results, we obtain an expression for the quadrupole signature arising from GI alignment and a shape-dependent selection bias:

$$\xi_{\text{GI}} = \langle Q(r) \rangle = \epsilon_{\text{LRG}} \frac{\tau}{3 \langle \epsilon_{zz}^2 \rangle} \int \frac{q^2 dq}{2\pi^2} P(q) j_2(qr) \quad (26)$$

GALAXIES ARE
POINTING AT EARTH???

6 MODELING DESI'S SELECTION EFFECTS

In Section 3 we measured how the shapes of galaxies projected onto the sky are aligned with the density field. To infer how this affects RSD measurements, we need to estimate the extent of DESI's orientation dependence. Since real galaxies have a higher surface brightness and are more likely to pass selection, we expect a selection bias along the LOS. The polarization ϵ_{LRG} (Equation 4) relative to the LOS.

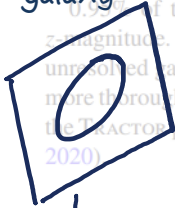
Well, there's a VERY small tendency for galaxies to be pointing at us. And it's only in the sample of galaxies that DESI has chosen to observe. We have a sample of LRGs which is similar to the sample described in Section 2.1, except without the fiber magnitude cut. We assign each parent LRG a 3D galaxy light profile, then simulate images of each profile from all viewing angles, without any extinction from internal dust. The polarization ϵ_{LOS} is defined as the ellipticity (Equation 4) relative to the LOS.



6.1 Parent Sample

We estimate polarization using a subsection of DESI LRGs in an area of the sky with the best-resolved shapes, with right ascension and declination between 0° and 180° and 0° and 90° . This area is in the South Galactic Cap (SGC) and part of the Legacy Imaging Survey (LIS) region. The parent sample of 41120 objects has the same criteria as DESI's main sample, with a total z-magnitude cut of $z_{\text{fiber}} < 21.61$ for the SGC. The fiber magnitude comes from the light within a 1'' aperture after convolving the shape model with a standardized PSF. This somewhat isolates the fiber magnitude from seeing variations, so we can safely use shapes from an area with the best seeing without impacting the distribution

2D picture of shapes. As in Section 2, we also use shape parameters from the best-fit, non-circular, model. 0.5% of this sample have the same fiber z-magnitude as total z-magnitude. This indicates that these objects are likely to be unselected galaxies. We ignored these objects for our analysis, a more thorough simulation would involve simulating galaxies through the TRACTOR pipeline, as is done with DESI (Vauglin et al. 2020).



6.2 Light Profiles

Our light profile for each galaxy begin as a realization of 100,000 points. This representation allows us to rapidly apply the triaxial axis lengths, rotation, and projection to the 3D shapes. We represent the PSF (by definition) and the eventual fiber by a 2D Gaussian.

The point positions for each galaxy are distributed in 3D based on its best-fit shape parameters from the parent catalog. DESI's TRACTOR pipeline represents selected galaxy shapes as a mixture of Gaussians (Hogg & Lang 2013). To de-project these into 3D, we take advantage of the fact that a 3D Gaussian projects onto a 2D Gaussian. Therefore, the 2D Gaussian mixture fits allow us to immediately construct a 3D model. This was done for all parent LRGs with a best-fit profile of Vaucouleurs, exponential, and round-exponential LRGs. Relative

see if the galaxy would pass selection if it was viewed from a different angle



generate 3D shape which matched the picture

measure the orientation of the galaxy if it passed

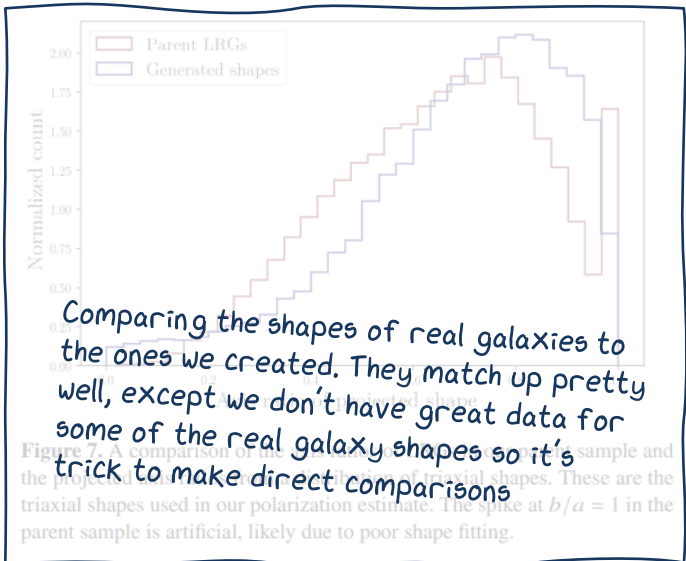


Figure 7. A comparison of the normalized count of triaxial shapes in the parent sample and the projected distribution of triaxial shapes. These are the triaxial shapes used in our polarization estimate. The spike at $b/a = 1$ in the parent sample is artificial, likely due to poor shape fitting.

few LRGs were fit best with a Sersic profile. These tend to be bright enough that they are not near the aperture magnitude cut and therefore less affected by this biased selection; for simplicity we modeled these with a Hernquist profile (Hernquist 1990).

6.3 Polarization Estimate

For each object in the parent sample, we assign a triaxial shape based on its properties. The shapes are randomly drawn from the expected distribution of triaxial shapes for bright ($M_r > -19$), medium ($-19 < M_r < -21$) and faint ($M_r > -21$) galaxies in imaging from the Sloan Digital Sky Survey (Balogh & Strauss 2008). 41120 3D shapes were projected along a random viewing angle and ranked by the axis ratio b/a . The parent sample was sorted by axis ratio and matched with the triaxial shape corresponding to the projected shape of the same rank.

To test these triaxial shapes, we viewed them each from a different angle and compared the projected axis ratios to our parent sample (Figure 7). These distributions are not identical; note the artificial spike in the parent sample at $b/a = 1$ which is likely from poor shape fitting. The difference in the distributions could also be due to shape-dependent fitting biases in TRACTOR, or imperfect distributions from Padma & Strauss (2008), including shape evolution from $z = 0$ or $z = 0.5$.

The point positions from Section 6.2 were scaled by the assigned triaxial axis lengths for each galaxy. They were then rotated to 100 random orientations and projected along one axis. The resulting ‘images’ were scaled using the ratio of the observed half-light radius and the average half-light radius of the parent sample. This was done to emulate an observation in 1'' seeing. Instead of convolving with a Gaussian, we used a deconvolution kernel to add the effects of 2D deflections to the projected points. The fiber magnitude was estimated by from the fraction of points which fell within an 1.5'' diameter aperture. The resulting 2D light profiles used did not perfectly replicate the observed z-fiber values, so we added a calibration factor to the N-body fiber magnitude for each of the four light profiles to match the true z-fiber median. The effects with a fiber magnitude less than 21.61 passed selection.

For each simulated image which passed selection, we measured the corresponding 3D profile several times. We then repeat several million times to measure the ellipticity relative to the LOS. This is the same convolution as Equation 4, except shapes are projected in the transverse direction. The average of these is our

Some pretty visualizations of the orientation bias in DESI's galaxies.

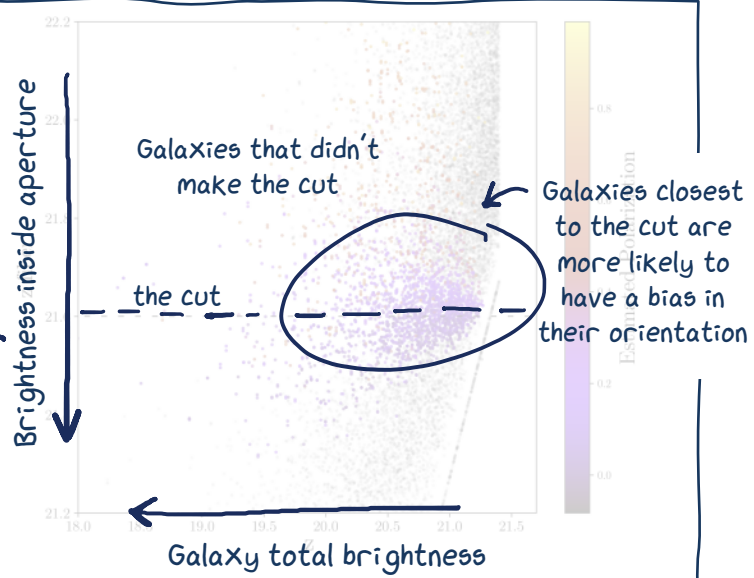
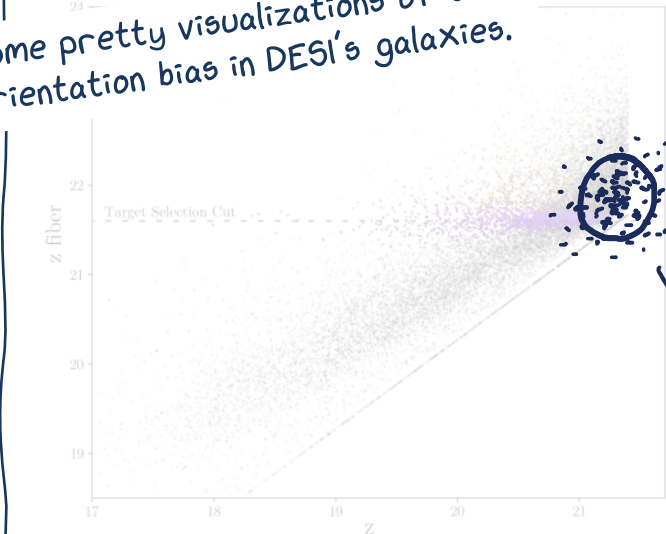


Figure 8. Results from our N-body reproduction of DESI's target selection. There are two main flux cuts on the LRG: a sliding $r - W1$ vs $W1$ cut which dominates at bluer colors, and the z_{fiber} cut which dominates at redder colors. The full parent sample is shown on the left, and a closer look near the fiber magnitude cut on the right. Each galaxy was assigned a triaxial shape, which was rotated to 100 random orientations. Its polarization is the average ellipticity relative to the light of sight of the objects which passed an aperture-magnitude cut. For target selection, we find that the orientation of shapes matters only for objects very close to the fiber magnitude cut, and is more likely to matter for more elliptical galaxies.

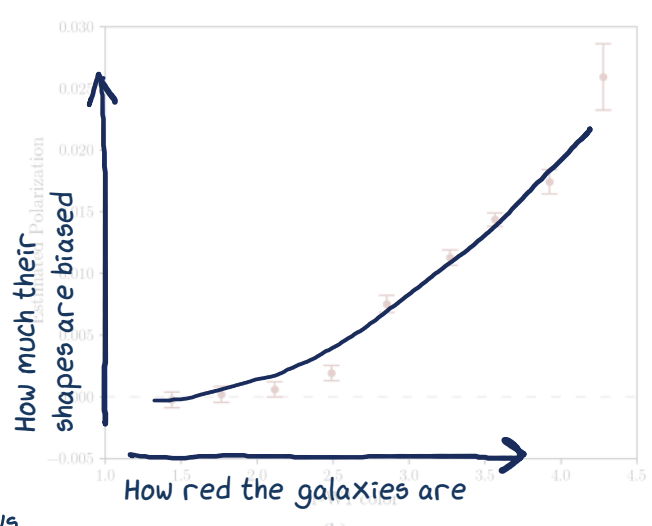


Figure 9. Properties of the targets from our simulation, as the z mag and color taken from a parent sample of LRGs. Each square is colored by the average polarization in that bin. We attribute the variation in polarization near the fiber-magnitude cut to a selection effect: in order for these targets to pass selection they must have a fiber magnitude very close to their total magnitude, i.e., they must have more compact shapes and a damped polarization. b: the polarization of selected targets binned by color. We expect this trend, since fainter galaxies tend to fall closer to the fiber-magnitude cut (Figure 8). A higher polarization for redder colors could lead to an increased ξ_2 bias at higher redshifts and mimic structure growth.

polarization $\epsilon_{\text{LRG}} = 54.2\%$ of our simulated galaxy images passed the fiber magnitude cut, similar to the actual value of 52.1%. The

polarization for these galaxies is 0.0087 ± 0.0002 . By determining the selection of a set of orientations for each galaxy shape, we can also estimate which galaxies in the original sample may have an orientation bias. To see what polarization DESI can measure for its targets, we've plotted the average polarization in bins of z mag and $r - W1$ color (Figure 9a).

We also find that the redder LRGs may be more affected by orientation bias than the bluer ones. This translates to a correlation between redshift and polarization if galaxies were sticks that all pointed at Earth

orientation, which could affect studies of structure evolution (Figure 9b).

7 ESTIMATE OF ξ_2 BIAS

At this point, we have measured all the necessary components to estimate the ξ_2 signature arising from IA and DESI's selection bias.

ϵ_{LRG} , the polarization of galaxy shapes along the LOS, is measured in Section 6. $\langle \epsilon_{zz}^2 \rangle$ is the variance of the real part of the complex ellipticities which describe the shapes of DESI's LRGs and is 0.031.

$$\epsilon_{zz} = 0.009$$

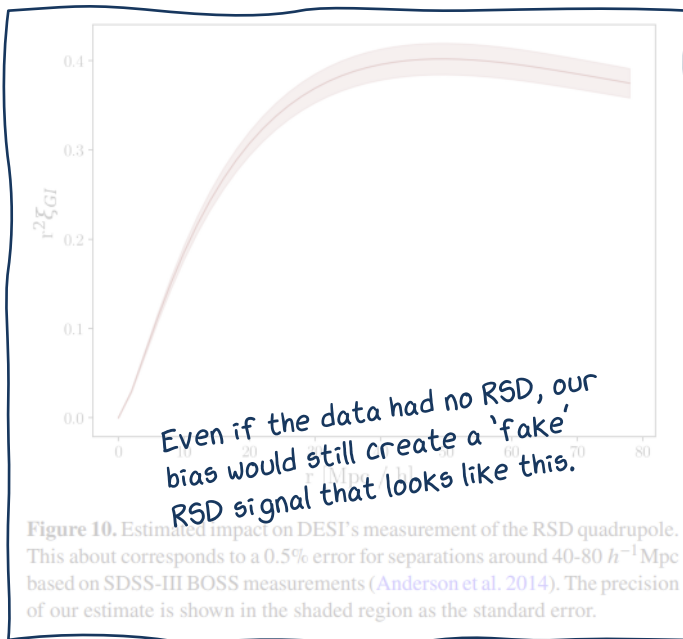


Figure 10. Estimated impact on DESI’s measurement of the RSD quadrupole. This about corresponds to a 0.5% error for separations around $40\text{--}80 h^{-1}\text{Mpc}$ based on SDSS-III BOSS measurements (Anderson et al. 2014). The precision of our estimate is shown in the shaded region as the standard error.

PUTTING IT ALL TOGETHER

We used the power spectrum, $P(K)$ from ABACUSUMMIT (Maksvig et al. 2021) as a function of effective depth L , or how far along the line of sight we average when measuring ϵ_{LRG} . This was estimated using the color weighting scheme from Section 3.2 to be $L = 865 h^{-1}\text{Mpc}$. It also depended on the projected comoving density fluctuations $\Delta w_x(r)$ which we measured in Section 3. Average over the bin of projected separation, we estimate $r_{\text{obs}} = -0.17$.

Using all the above components put together, we determine $r^2 \xi_{GI}$ to be $3.5 h^{-1}\text{Mpc}$ around $10\text{--}80 h^{-1}\text{Mpc}$. The full separation dependence is shown in Figure 10. SDSS-III measures ξ_2 at $10\text{--}80 h^{-1}\text{Mpc}$ (Anderson et al. 2014). We predict that DESI’s measurements of RSD will be lowered by about 0.5% at $80 h^{-1}\text{Mpc}$.

8 ξ_2 BIAS WITH ABACUS

REPRODUCING EVERYTHING WITH THE SIMULATION

Reproducing everything in the simulation produces a false ξ_2 signature and test our linear ξ_2 - w_x model connecting the GI and RSD signals. We can solve this problem using ABACUS SUMMIT simulations.

As in Section 4, we started with a $2000 h^{-1}\text{Mpc}$ box of large halos and mapped their positions to redshift, right ascension, and declination. Sky cuts were applied to ensure a uniform sky distribution at each redshift. 3D Sersic profiles of 100,000 points were generated for each halo, as in Sections 6.2–6.3, except using the halo’s original triaxiality. The points were randomly distributed as drawn from a distribution matching the physical radii of the DESI LRG parent sample and scaled using the average half-light radius of the point profile. In each LRG parent sample, we counted the number of points which fell within a $1.75''$ aperture and measured the shape of each halo projected onto the sky and relative to the LRG.

But how can we be sure that our equations are spitting out the right answer? One way to do a reality check is with the simulated universe from before.

To see how an aperture selection impacts the ξ_2 measurement, we created two samples: one without any selection, and one only with halos containing more than 48,000 points within the aperture, which corresponds to 50% of the halos. We measured $\xi_2(r)$ for both in real space and in redshift space using the halo’s original orientation and determined using the Landy-Szalay Estimator (Landy

We’re so close to figuring out the question...

...determined using the Landy-Szalay Estimator (Landy

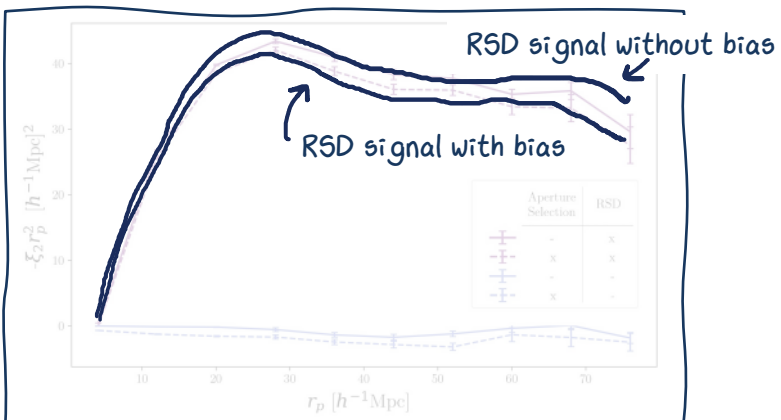


Figure 11. Results from reproducing our measurements with a simulation. The two lines include Redshift-Space Distortions. The aperture-based selection creates an artificial, non-zero RSD signature, which acts in opposition to ξ_2 on large scales.

& Szalay 1993) and averaged over 10 sets of randoms, generated with random right ascension and declinations for each redshift. This entire process is done for each of the 156 redshift bins, and their average $\xi_2(0)$ and standard error is shown in Figure 11.

We use the simulation to create fake data, then measure the RSD signal before and after we apply the target selection which biases orientations.

As in Section 7, we used our linear model to predict the ξ_2 bias caused by the target selection. We measured the projected intrinsic alignment of the halo catalog in radial bins which resulted in a effective depth of $156 h^{-1}\text{Mpc}$. The polarization due to aperture cut was $\epsilon_{LRG} = 7.6 \pm 0.1 \times 10^{-3}$. The resulting prediction is compared to the model in Figure 12.

We expect the bulk of the disagreement between these two simple models to be due to the linear approximation, which does not hold at lower separations, and simplifications in the demonstration mock.

We also compare this to what our equations predict would be the RSD bias for this fake data (result in plot on next page).

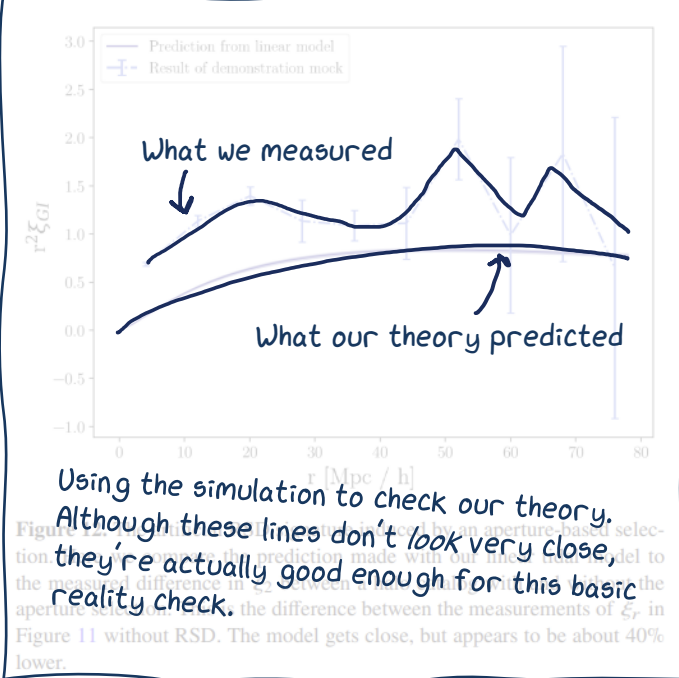
9 CONCLUSION

The main goal of this study is to determine the approximate impact on DESI’s RSD measurements due to an orientation bias in LRGs. We have demonstrated that the effect is significant for DESI and estimate a 0.5% fractional decrease of ξ_2 for separations of $10\text{--}80 h^{-1}\text{Mpc}$. DESI forecasts a total $f\sigma_8$ around 0.4–0.7% (with ELG and LRGs combined), so this is a significant fraction of the total error.

But how can we be sure that our equations are spitting out the right answer? One way to do a reality check is with the simulated universe from before. To reduce the effects of intrinsic alignment for DESI, simple yet severe choices involve only measuring ξ_2 in galaxy subsamples, perhaps cut by total polarization. Alternatively, our estimate could be used for calibration.

As the DESI survey progresses and the precision in ξ_2 increases, there are several opportunities to improve our bias estimate. Our estimate is directly proportional to the measured polarization ϵ_{LRG} and RSD signal w_x , both of which include systematic uncertainties. The main uncertainty comes from the choice of the triaxial shape distribution. We expect the majority of our galaxies to be prolate (Padmanabhan & Trivedi 2017), which are more favored by the Landy-Szalay estimator than oblate, and result in a higher polarization. We match the expected distribution of projected shapes in a region of the sky with the best shape fits, but 5.6% of galaxies

continued



in this subsample are fit as circles, creating an artificial spike at $b/d = 1$ (Figure 7). A better estimate could be made with more accurate shapes, i.e. from the Dark Energy Survey (Gatti et al. 2021), although this would add significant uncertainty to the model's predictions. Although partially mitigated by color weighting, the IA signal in this work is reduced by weak lensing and diluted by the inclusion of LRGs that have no redshift information. This will be drastically improved with DESI's first year of data, which contains 2.5 million quality LRG spectra. The LOS distance we average over has a 10% uncertainty in radial distances, $L \approx 865 h^{-1} \text{ Mpc}$, which increases the factor of at least 20 with redshifts. Advances in our ability to measure IA for only pairs of LRGs, which are physically associated with the strongest sources of bias in the bias ξ_{IA} , will further improve this.

ACKNOWLEDGEMENTS

CL wishes to acknowledge Sean Moss for his support, software and otherwise, and Tanveer Karim for many helpful conversations. The authors also thank Eric Jullo, Eusebio Sanchez, Robert Kehoe, and Zachary Slepian for their input through the collaboration review process.

This material is based upon work supported by the National Science Foundation Graduate Research Fellowship under Grant No. DGE1745303, the U.S. Department of Energy under grant DE-SC0013718, and NASA under ROSES grant 12-EUCLID12-0004. DJE is further supported by the Simons Foundation.

It takes many individuals, institutions, and funding agencies to make a project like DESI happen!
This research is also supported by the Director, Office of Science, Office of High Energy Physics, U.S. Department of Energy under Contract No. DE-AC02-05CH11231, and by the National Energy Research Scientific Computing Center, a DOE Office of Science User Facility. In fact; additional support for DESI is provided by the U.S. National Science Foundation, Division of Astronomical Sciences under Contract No. AST-0950945 to the NSF's National Optical-Infrared Astronomy Research Laboratory; the Science and Technologies Facilities Council of the United Kingdom; the Gordon and Betty Moore Foundation; the Heising-Simons Foundation; the French Alternative Energies and Atomic

In the conclusion, we're also very careful to explain assumptions we made. The point of this paper is mainly to get an estimate of how big this effect will be for DESI.

The DESI Legacy Imaging Surveys consist of three individual and complementary projects: the Dark Energy Camera Legacy Survey (DECaLS), the Beijing-Arizona Sky Survey (BASS), and the Mayall z-band Legacy Survey (MzLS). DECaLS, BASS and MzLS together include data obtained, respectively, at the Blanco telescope, Cerro Tololo Inter-American Observatory, NSF's NOIRLab; the Bok telescope, Steward Observatory, University of Arizona; and the Mayall telescope, Kitt Peak National Observatory, NOIRLab. NOIRLab is operated by the Association of Universities for Research in Astronomy (AURA) on behalf of the National Science Foundation. Pipeline processing and analyses of the data were supported by NOIRLab and the Lawrence Berkeley National Laboratory. Legacy Surveys also uses data products from the Near-Earth Object Wide-field Infrared Survey Explorer (NEOWISE), a project of the Jet Propulsion Laboratory/California Institute of Technology, funded by the National Aeronautics and Space Administration. Legacy surveys are funded by the U.S. Department of Energy, the National Energy Research Scientific Computing Center, a DOE Office of Science User Facility; the U.S. National Science Foundation, Division of Astronomical Sciences; the National Astronomical Observatories of China, the Chinese Academy of Sciences and the Chinese National Natural Science Foundation. This is managed by the Regents of the University of California under contract to the U.S. Department of Energy. The complete acknowledgement can be found at <https://www.legacysurveys.org/>.

The author(s) are honored to be permitted to conduct scientific research on Ma'aleh Hagag (Cat Peak), a mountain of great significance to the Tohono O'odham Nation. All data from the DESI Legacy Imaging Survey is publicly available at legacysurvey.org. CatalogSummaries and other data products are publicly available at abacus.uchicago.edu. Generating ellipsoids and generating light profiles can be done at github.com/cmlamman/ellipse_alignment.

REFERENCES

- I DIDN'T START FROM SCRATCH**
I. D. Mandelbaum, et al., 2017, Technical report, Overview of the Instrumentation for the Dark Energy Spectroscopic Instrument, <https://ui.adsabs.harvard.edu/abs/2022arXiv220510939A>. Lawrence Berkeley National Laboratory, <https://ui.adsabs.harvard.edu/abs/2022arXiv220510939A>.
Anderson L. C., et al., 2014, *Nature*, 509, 337. Royal Society, 441, 24.
Binney J., 1985, *Monthly Notices of the Royal Astronomical Society*, 212, 767.
Catelan P., Porciani C., 2001, *Monthly Notices of the Royal Astronomical Society*, 321, 113.
Collaboration P., et al., 2020, *Astronomy and Astrophysics*, 641, A6.
DESI Collaboration et al., 2016, Technical report, The DESI Experiment Part II: Instrument Design, <https://ui.adsabs.harvard.edu/abs/2016arXiv161100037D>. Lawrence Berkeley National Laboratory, <https://ui.adsabs.harvard.edu/abs/2016arXiv161100037D>.
Dey A., et al., 2019, *The Astronomical Journal*, 157, 168.

- Gatti M., et al., 2021, *Monthly Notices of the Royal Astronomical Society*, 504, 4312
- Gendzwill D. J., Stauffer M. R., 1981, *Journal of the International Association for Mathematical Geology*, 13, 135
- Hadzhiyska B., Eisenstein D., Bose S., Garrison L. H., Maksimova N., 2021, *Monthly Notices of the Royal Astronomical Society*, 509, 501
- Hernquist L., 1990, *The Astrophysical Journal*, 356, 359
- Hirata C. M., 2009, *Monthly Notices of the Royal Astronomical Society*, 399, 1074
- Hirata C. M., Seljak U., 2004, *Physical Review D*, 70, 063526
- Hirata C. M., Mandelbaum R., Ishak M., Seljak U., Nichol R., Pimbblet K. A., Ross N. P., Wake D., 2007, *Monthly Notices of the Royal Astronomical Society*, 381, 1197
- Hogg D. W., Lang D., 2013, *Publications of the Astronomical Society of the Pacific*, 125, 719
- Jackson J. C., 1972, *Monthly Notices of the Royal Astronomical Society*, 156, 1P
- Kaiser N., 1987, *Monthly Notices of the Royal Astronomical Society*, 227, 1
- Kitanidis E., et al., 2020, *Monthly Notices of the Royal Astronomical Society*, 496, 2262
- Kong H., et al., 2020, *Monthly Notices of the Royal Astronomical Society*, 499, 3943
- Landy S. D., Szalay A. S., 1993, *The Astrophysical Journal*, 412, 64
- Lang D., Hogg D. W., Mykytyn D., 2016, *Astrophysics Source Code Library*, p. ascl:1604.008
- Maksimova N. A., Garrison L. H., Eisenstein D. J., Hadzhiyska B., Satterthwaite T. P., 2021, *Monthly Notices of the Royal Astronomical Society*, 508, 4017
- Martens D., Hirata C. M., Ross A. J., Fang X., 2018, *Monthly Notices of the Royal Astronomical Society*, 478, 711
- Obuljen A., Percival W. J., Dalal N., 2020, *Journal of Cosmology and Astroparticle Physics*, 2020, 058
- Padilla N. D., Strauss M. A., 2008, *Monthly Notices of the Royal Astronomical Society*, 388, 1321
- Singh S., Mandelbaum R., More S., 2015, *Monthly Notices of the Royal Astronomical Society*, 450, 2195
- Singh S., Yu B., Seljak U., 2021, *Monthly Notices of the Royal Astronomical Society*, 501, 4167
- Tenneti A., Mandelbaum R., Di Matteo T., Feng Y., Khandai N., 2014, *Monthly Notices of the Royal Astronomical Society*, 441, 470
- Troxel M. A., Ishak M., 2015, *Physics Reports*, 558, 1
- Zhou R., et al., 2021, *Monthly Notices of the Royal Astronomical Society*, 501, 3309



To learn more about DESI,
check out desi.lbl.gov

If you've gotten this far, CONGRATULATIONS!
I hope my notes made it easier to digest this
paper. If you're a scientist, I would love to
read similar notes on one of your papers :)

I made this in power point using the XKCD font:
<https://github.com/ipython/xkcd-font>



APPENDIX A: PROJECTION OF TRIAXIAL ELLIPSOIDS

This section details how we obtained the axis ratios and orientations of projected triaxial ellipsoids for our mock $\text{M}_87\gamma$ s. We adapted the method derived in Gendzwill & Stauffer (1981) to project ellipsoids onto the celestial sphere.

Welcome to the part of my paper I'm most proud of. We define the diagonal matrix Γ such that $\Gamma_{ij} = \delta_{ij}\lambda_j^{-2}$, where δ is a Kronecker delta. We denote the primary axis directions \vec{s}_j and organize them as rows of a matrix \mathbf{S} , so that S_{ij} is the j^{th} component of the i^{th} vector. We are projecting along the \hat{x} unit vector direction, here denoted as component 1, onto the $\hat{y} - \hat{z}$ plane.

We define the column vector \vec{m} as

$$\vec{m} = (\hat{x}^T \mathbf{S}^T \Gamma \mathbf{S} \hat{x})^{-1} \hat{x}^T \mathbf{S}^T \Gamma \mathbf{S} \quad (\text{A1})$$

where the pre-factor adopts the normalization that $\vec{m} \cdot \hat{x} = 1$. We then compute vectors \vec{u} and \vec{v} with elements $u_j = \hat{y} \cdot (\vec{m} \times \vec{s}_j)$ and $v_j = \hat{z} \cdot (\vec{m} \times \vec{s}_j)$, written alternatively as

$$\begin{aligned} u_j &= m_1 S_{j3} - m_3 S_{j1} \\ v_j &= m_1 S_{j2} - m_2 S_{j1} \end{aligned} \quad (\text{A2})$$

We use these to compute the scalars $A = \vec{u}^T \Gamma \vec{u}$, $B = \vec{u}^T \Gamma \vec{v}$, and $C = \vec{v}^T \Gamma \vec{v}$.

The orientation angle of the projected ellipse's primary axis, measured in the $+\hat{y}$ direction from \hat{z} is

$$\tan 2\theta = \frac{-2B}{A-C} \quad (\text{A3})$$

I found a great reference in a geology paper from 1981!

They needed to know what shape a 3D rock would have when you cut through it.

$$\begin{aligned} \frac{1}{a^2} &= \frac{A+C}{2} + \frac{A-C}{2 \cos 2\theta} \\ \frac{1}{b^2} &= A + C - \frac{1}{a^2} \end{aligned} \quad (\text{A4})$$



I adapted their method for galaxies, and present it here in a very clean way (I hope)!

APPENDIX B: EXPANDED DERIVATIONS

B1 Shape-Density Correlation

Starting from Equation 16, we can continue the computation as:

$$w_{\times}(R) = \frac{\tau}{L} \int dz \int \frac{d^3q}{(2\pi)^3} \left[\frac{q_x^2/3 - q_y^2}{q^2} \right] e^{-i\vec{q} \cdot \vec{x}} \Big|_{\vec{x}=0} \int \frac{d^3k}{(2\pi)^3} e^{i\vec{k} \cdot \vec{r}} \Big|_{\vec{r}=(R,0,z)} \langle \tilde{\rho}^*(\vec{q}) \tilde{\rho}(\vec{k}) \rangle \quad (\text{B1})$$

$$= \frac{\tau}{L} \int dz \int \frac{d^3k}{(2\pi)^3} \left[\frac{k_x^2}{3} - k_y^2 \right] k^{-2} P(k) e^{i\vec{k} \cdot \vec{r}} \Big|_{\vec{r}=(R,0,z)}. \quad (\text{B2})$$

Next, the integral over z creates $\int dz \exp(ik_z z) = (2\pi)\delta^D(k_z)$. We denote the space of (k_x, k_y) as \vec{K} , and similarly \vec{R} as (x, y) . So we have

$$w_{\times}(R) = \frac{\tau}{L} \int \frac{d^2K}{(2\pi)^2} \left(\frac{K_x^2}{3} - K_y^2 \right) K^{-2} P(K) e^{i\vec{K} \cdot \vec{R}}. \quad (\text{B3})$$

To simplify this, we introduce

$$\Phi(\vec{R}) = \int \frac{d^2K}{(2\pi)^2} \frac{P(K)}{K^2} e^{i\vec{K} \cdot \vec{R}}, \quad (\text{B4})$$

which in turn implies

$$w_{\times}(R) = \frac{\tau}{3L} \left(2\partial_y^2 - \partial_x^2 \right) \Phi(\vec{R}) \Big|_{\vec{R}=R\hat{x}}. \quad (\text{B5})$$

$\Phi(\vec{R})$ is isotropic, and can be simplified to a Hankel transform

$$\Phi(R) = \int \frac{K dK}{2\pi} \frac{P(K)}{K^2} J_0(KR) \quad (\text{B6})$$

with J_0 being the Bessel function. For a general function $f(R)$, we have $\partial^2 f / \partial x^2 = \partial^2 f / \partial R^2$ and $\partial^2 f / \partial y^2 = (1/R) \partial f / \partial R$. So we have

$$w_{\times}(R) = \frac{\tau}{3L} \left(\frac{2}{R} \partial_R - \partial_R^2 \right) \Phi(R) = \frac{\tau}{3L} R^2 \frac{d}{dR} \left[\frac{1}{R^2} \Psi(R) \right] \quad (\text{B7})$$

where we introduce

$$\Psi(R) = -\frac{d\Phi}{dR} = \int \frac{K}{2\pi} \frac{dK}{K} \frac{P(K)}{K} J_1(KR), \quad (\text{B8})$$

using $dJ_0(x)/dx = J_1(x)$.

B2 Shape - ξ_2 Correlation

Details of the derivation of Equation 22

Using $L_2(\mu) = (3/2)\mu^2 - (1/2)$,

$$q_z^2 - \frac{q^2}{3} = q^2 \left(\mu_q^2 - \frac{1}{3} \right) = \frac{2q^2}{3} L_2(\mu_q) \quad (\text{B9})$$

for a 3-d vector \vec{q} , and $L_\ell = \sqrt{4\pi/(2\ell+1)}Y_{\ell 0}$. We note that

$$\frac{T_{zz}}{2} = \frac{1}{3} \int \frac{d^3 k}{(2\pi)^3} L_2(\mu_k) \tilde{\rho}(\vec{k}) e^{i\vec{k}\cdot\vec{r}}. \quad (\text{B10})$$

Finally, we have the expansion of a plane wave into spherical harmonics and spherical Bessel functions:

$$e^{i\vec{q}\cdot\vec{r}} = 4\pi \sum_{\ell m} i^\ell j_\ell(qr) Y_{\ell m}^*(\hat{q}) Y_{\ell m}(\hat{r}). \quad (\text{B11})$$

We then compute $\langle \epsilon_{zz} Q(r) \rangle$ as

$$\langle \epsilon_{zz} Q(r) \rangle = 5\tau \int \frac{d^3 q}{(2\pi)^3} \frac{1}{3} L_2(\hat{q}) \int \frac{d^2 \hat{r}}{4\pi} L_2(\hat{r}) \int \frac{d^3 k}{(2\pi)^3} e^{i\vec{q}\cdot\vec{r}} \langle \tilde{\rho}^*(\vec{q}) \tilde{\rho}(\vec{k}) \rangle \quad (\text{B12})$$

Converting to power, doing the \vec{k} integral, and expanding the plane wave yields

$$\langle \epsilon_{zz} Q(r) \rangle = \frac{5\tau}{3} \int \frac{q^2 dq}{2\pi^2} P(q) \int \frac{d^2 \hat{q}}{4\pi} L_2(\hat{q}) \int \frac{d^2 \hat{r}}{4\pi} L_2(\hat{r}) 4\pi \sum_{\ell m} i^\ell j_\ell(qr) Y_{\ell m}^*(\hat{q}) Y_{\ell m}(\hat{r}). \quad (\text{B13})$$

We then can do the two angular integrals, yielding the simpler form:

$$\langle \epsilon_{zz} Q(r) \rangle = -\frac{\tau}{3} \int \frac{q^2 dq}{2\pi^2} P(q) j_2(qr). \quad (\text{B14})$$

This paper has been typeset from a $\text{\TeX}/\text{\LaTeX}$ file prepared by the author.

Alright, this is actually the end.

